The 7th IEEE International Conference on E-Health and Bioengineering - EHB 2019
Grigore T. Popa University of Medicine and Pharmacy, Iasi, Romania, November 21-23, 2019

Hyperspectral Image Classification using the MRELBP Texture Descriptor

Stefania Barburiceanu, Romulus Terebes, Serban Meza
Communications Department, Technical University of Cluj-Napoca, Cluj-Napoca, Romania
Email addresses: Stefania.Barburiceanu@com.utcluj.ro, Romulus.Terebes@com.utcluj.ro, Serban.Meza@com.utcluj.ro

***Abstract*—This paper presents an extension of the Local Binary Patterns feature descriptors to hyperspectral image classification. Our approach uses a Principal Component Analysis technique to extract the most representative bands and for each pixel, it concatenates the histograms obtained for each selected band. The histograms are built from features which are discriminative and invariant to different transformations in the input. The proposed method achieves promising results for hyperspectral image classification. We tested our technique on four publicly available hyperspectral image databases of Earth observation images and for all of them the proposed method improved the classification accuracy when compared to the classical Local Binary Pattern approach.**

Keywords—hyperspectral image classification, Local Binary Patterns, feature extraction

I. Introduction

Image classification represents one of the most important fields in computer vision, being widely used in the medical domain and in remote sensing and industrial applications. This process involves the prediction of a category for a given image. In the supervised classification case, there are always two steps: training and testing. The first step involves using a training set which contains training image samples and the categories they belong to. The goal of this step is to generate a model by extracting relevant features from the training images in order to obtain an efficient and discriminative description. In the testing stage, an unknown image sample is used as input for the classification system. The new sample is also analysed by extracting relevant characteristics using the same feature extraction method as for the training step. By using these features and the created model, the category for the new sample is predicted. Two techniques are used in the supervised classification system: feature extraction and machine learning classification. Feature extraction is the most important process for image classification, involving the extraction of relevant and discriminative characteristics from raw images. Image classification is sometimes a difficult task due to the variable conditions to which images are exposed: lighting, observation scales, rotation and noise. In order to achieve a consistently good classification performance, the extracted features must be invariant to these conditions.

Due to recent advances in hyperspectral sensor technology, there is a need to develop new feature extraction methods specifically adapted to hyperspectral images in which data is represented as image cubes. These types of data contain many narrow spectral bands that provide rich spectral information. Instead of providing only spatial information from the visible spectrum, hyperspectral imaging uses also the electromagnetic radiation from outside the visible spectrum, such as the ultraviolet and infrared bands. This can improve the discrimination power over human visual system replicated methods because the latter can perceive some materials as being identical, even if they have in fact different characteristics in the infrared or ultraviolet spectra.

The LBP (Local Binary Patterns) operator [1] attracted many researchers because of its computational simplicity, illumination invariance and its good performance in texture classification. The original formulation was extended in [2] to become invariant to rotation and observation scale by using circular neighbourhoods of variable sizes. The same paper introduces the uniform patterns concept and the multiresolution approach. It was stated in [2] that a greater number of spatial transitions in a pattern involves a higher probability that the pattern will change to a different one due to rotation. Also, some patterns occur more frequently than others in textures and the usage of all patterns can reduce the performance, both in terms of processing times and in accuracy. Based on this argument, the authors in [2] introduce the uniform patterns, those patterns in which there are at most two bitwise transitions. In the same publication, the multiresolution approach was also put forward. It involves capturing information from several scales and performing a histogram concatenation. For improving the discrimination power of the extracted features, many LBP versions were proposed, one being the ELBP (Extended Local Binary Pattern) operator [3]. However, this descriptor is very sensitive to noise. In order to increase the noise tolerance of the ELBP descriptor, the MRELBP (Median Robust Extended Local Binary Patterns) operator was introduced in [4].

Since hyperspectral images are a special case of multi 2D images, the feature extraction methods should be adapted to deal with this type of data. Different extensions of LBP operators to 3D were proposed in literature, such as considering a sphere instead of a circle for defining a central voxel and its neighbours [5]. Another extension to 3D proposed in [6] is based on the pre-computation of some 2-patterns followed by the dot-product with a threshold. Sen Jia et al. considered a 3D regular octahedral to compute the LBP values and formed eight patterns groups to ensure rotation invariance for hyperspectral image classification [7]. Another LBP adaptation to hyperspectral images involves the concatenation of histograms obtained from three orthogonal planes [8].

We propose an extension of the MRELBP descriptor [4] to hyperspectral images. The MRELBP operator proved to generate characteristics that offer exceptional performance for texture classification, being invariant to illumination conditions

978-1-7281-2603-6/19/$31.00 ©2019 IEEE

and to rotation. It offers also a degree of invariance to the observation scale change by using a multiresolution strategy and it is also described by the authors in [4] as being robust to noise. This paper proposes a new way of using the MRELBP operator for extracting spatial-spectral features for hyperspectral image classification. Since in hyperspectral imagery there are hundreds of spectral bands and some of them are not relevant for the classification process, a band reduction is performed by using a Principal Component Analysis technique. For each selected spectral band, a MRELBP code is obtained. Then, for each pixel of the input image, a small patch around it from the MRELBP codes is considered. A histogram is calculated from the values comprised in this neighbourhood. The concatenation of the computed histograms for each spectral band is considered as feature vector.

II. Related work

A. Local Binary Patterns

The original LBP operator [1] produces a local representation of grey-level textures by transforming the input image in a feature vector. The local representation is obtained by a comparison between each pixel (central pixel x_c) and its P neighbours (P=8 for the original formulation) and the resulting 8-bit number is converted to decimal. The original LBP operator is calculated by using (1):

$$LBP_8(x_c)=\sum_{k=0}^{7} s(x_k - x_c)*2^k, \quad (1)$$

where *s(x)* is given in (2), x_k is the k^{th} neighbour and subscript 8 denotes the number of neighbours used:

$$s(x)=\begin{cases}0, \text{ si } x<0\\ 1, \text{ si } x\geq 0\end{cases} \quad (2)$$

This process is repeated for each pixel of the input image and finally the histogram of the LBP codes is considered as a feature vector describing the analysed texture.

The operator was extended [2] for being able to use circular neighbourhoods of different sizes, with different numbers of neighbours. In this case, some values do not fall exactly at integer pixel coordinates and are estimated by bilinear interpolation. The authors also introduce the notion of uniform patterns which correspond to those patterns where the number of spatial transitions is at most 2. As pointed out in [2], a smaller number of transitions is more likely to ensure rotation invariance than a higher number. The uniform patterns are labelled separately in *P+1* categories (the label corresponds to the number of unitary bits) and the non-uniform patterns are grouped together under the label *P+1*, the final histogram having *P+2* bins. The extended operator is defined in (3):

$$LBP^{riu2}_{R,P}(x_c)=\begin{cases}\sum_{k=0}^{P-1} s(x_c - x_{R,P,k}), \text{ if } U(LBP_{R,P})\leq 2\\ P+1, \text{ otherwise}\end{cases}, \quad (3)$$

where $x_{R,P,k}$ is the k^{th} neighbour in a neighbourhood of radius *R* and *P* neighbours, *U()* is the uniformity function that calculates the number of bit-wise transitions and the superscript *riu2* shows the use of uniform rotation invariant patterns having the *U* value at most 2.

B. Median Robust Extended Local Binary Patterns

The MRELBP operator [4] is derived from the ELBP descriptor [3] which is very vulnerable to noise. In order to handle noise, Li Liu et al. use in [4] responses of a median filter which is applied on image neighbourhoods instead of raw pixel intensities. Two types of characteristics are used: pixel intensities and differences in pixel intensities. Two operators are built using the pixel intensities characteristics: MRELBP_CI (MRELBP Central pixel's Intensity) and MRELBP_NI (MRELBP Neighbours' Intensities) given in (4) and (5) respectively.

$$MRELBP\_CI(x_c)=s(\varphi(X_{c,w})-\mu_w)), \quad (4)$$

where $\varphi(X)$ represents the median value of *X*, $X_{c,w}$ is a neighbourhood of size $w * w$ centered on the central pixel x_c, μ_w is the average of $\varphi(X_{c,w})$ over the entire image and *s(x)* is the sign function given in (2).

$$MRELBP\_NI_{R,P}(x_c)=\sum_{k=0}^{P-1} s(\varphi(X_{R,P,w_R,k})-\mu_{R,P,w_R}))*2^k \quad (5)$$

where μ_{R,P,w_R} is defined in (6), $X_{R,P,w_R,k}$ is the neighbourhood of size $w_R * w_R$ centered on the neighbouring pixel $x_{R,P,k}$ and *P* is the number of neighbours:

$$\mu_{R,P,w_R}=\frac{1}{P} * \sum_{k=0}^{P-1} \varphi(X_{R,P,w_R,k}) . \quad (6)$$

The third operator uses differences between pixels' intensities on 2 circles centered on the central pixel and having the radii R and R ', R' <R. It is denoted MRELBP_RD (MRELBP Radial Difference) and is defined in (7):

$$MRELBP\_RD_{R,R-1,P,w_R,w_{R-1}}(x_c)=$$

$$\sum_{k=0}^{P-1} s(\varphi(X_{R,P,w_R,k})- \varphi\left(X_{R-1,P,w_{R-1},k}\right))*2^k . \quad (7)$$

III. Proposed approach

The proposed classification method involves the extraction of relevant features and a classic machine learning classification step. The workflow of the analysis method is similar to the one proposed in [9], including a band selection step, the extraction of relevant information and a fusion step.

1) Feature extraction

Through feature extraction, a feature vector matrix (containing the computed feature vector for each pixel of the input image) is obtained. It involves several steps: band reduction, the extraction of MRELBP codes, the histogram generation and the final feature vector matrix computation.

a) Band reduction

Hyperspectral images contain hundreds of spectral bands and even if the rich spectral information they provide is beneficial in the classification process, the huge amount of data can lead to very long processing times. For reducing the computational complexity, band reduction techniques are used to keep only the most representative and necessary spectral bands. One of the most popular approaches for dimensionality reduction is the Principal Component Analysis technique (PCA). It transforms a large dataset into a smaller one by

preserving most of the information contained in the initial set. If the variables in the initial set are correlated, they contain redundant information. The scope of this technique is to generate uncorrelated variables which contain as much information as possible from the initial variables, the principal components. A hyperspectral image contains several regions where pixels are expected to be of the same class. The PCA method takes the whole hyperspectral image and generates the principal components without taking into account the differences between different homogeneous regions and by using only the spectral information. For handling this problem, the authors in [10] propose the SuperPCA (superpixelwise PCA) technique. It involves a superpixel segmentation that generates homogeneous regions, the application of the PCA method on each one for extracting the same number of principal components and combining them to achieve a reduced hyperspectral image. In this paper, we propose the usage of the SuperPCA method for band reduction with B=10 principal components.

b) Extraction of MRELBP codes

The second step involves the extraction of MRELBP codes from the input image which is a hyperspectral cube with B bands. In order to achieve invariance to the change of the observation scale, 4 different radii were used in the computation of the *MRELBP* operators: 2, 4, 6 and 8. This choice is a compromise between the computational time and the discrimination power. The input image is a 3D cube, so the computation is performed for each band separately. For each radius and for each band, 3 operators are determined: *MRELBP_CI*, *MRELBP_NI* and *MRELBP_RD*. The median filter is applied on each band separately. The window size used for the *MRELBP_CI* operator is $w = 3$ and w_R is chosen according to the used radius: $w_R = R + 1$ as this setup achieved the best results [4]. In order to reduce the number of histogram bins, we keep the number of neighbours constant for all radii: $P = 8$. The mapping used is *riu2*. The *MRELBP_CI* operator has 2 possible values: 0 and 1. The *MRELBP_NI* and *MRELBP_RD* operators have 10 possible values each. After this step, we obtained 12 (for each of the 3 operators and for each of the 4 radii) three dimensional matrices of the same size as the input hyperspectral image.

c) Histogram generation

From the obtained MRELBP codes, for each pixel of the input image we computed histograms. For a given band, a given radius and obtained MRELBP code, we considered for each pixel a small patch around it of size 17*17 as it achieves the best performance as stated in [11]. The histogram was computed from the values contained in this neighbourhood. Fig. 1 shows the principle of pixel-wise histogram generation.

d) Feature vector computation

For a given band and for each pixel, we obtained 12 histograms: for each of the 3 operators and for each of the 4 scales of interest. The first step was to generate for a given band, for each pixel and for each scale a joint histogram denoted CINIRD (built from the CI - Central pixel's Intensity, NI - Neighbours' Intensities and RD – Radial Difference operators) by combining the obtained histograms for the 3 operators. The joint histogram has 10*10*2=200 values. Then, for each pixel, we concatenated the histograms obtained for each scale. Fig. 2 shows the feature vector computation for a given band. The final step is the concatenation of the feature vectors obtained for each band. All feature vectors are stored in a feature vector matrix which contains the values obtained for all pixels in the input image.

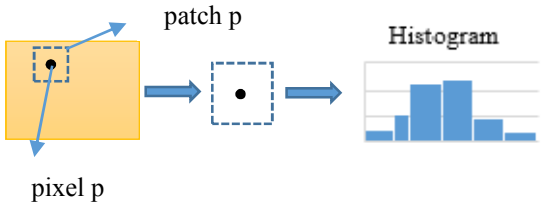

Fig. 1. Histogram calculation for a given radius, a given band and MRELBP operator

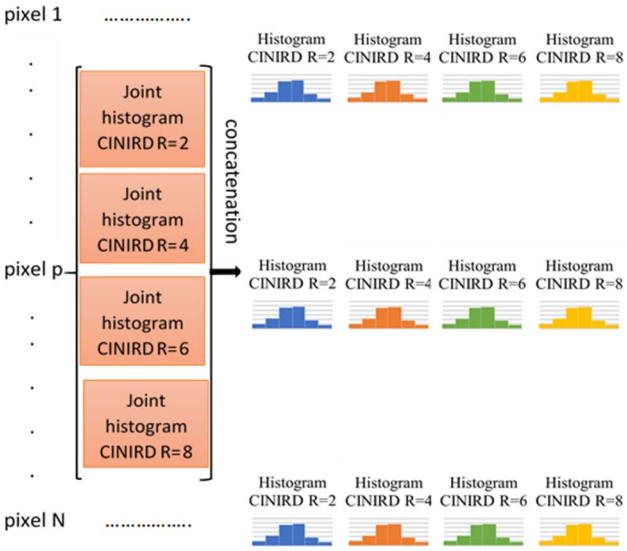

Fig. 2. Feature vector computation for a given band

2) Pixel-wise classification

For the classification step, we employed a Support Vector Machine (SVM) classifier with polynomial kernel. This technique is a complex machine learning algorithm which finds the optimal hyperplane (the one with the highest margin) that separates the predefined categories [12].

IV. Experimental Results

A. Databases

For evaluating the performance of the proposed classification method, we used four publicly available hyperspectral image databases: *Indian Pines, Salinas, Salinas A* and *Pavia University* [13]. For all databases, we did not consider the pixels from the background (labelled as category "0") and also some pixels nearby the image edges as we could not calculate the descriptors due to the lack of neighbours. We used 100 random partitions of the learning and test sets to calculate the mean accuracy and the associated standard deviation for all datasets.

B. Results

We tested the performance of the proposed classification method in comparison to the one obtained by using the rotation invariant uniform LBP operator with 8 neighbours and unitary radius extended to hyperspectral images [7]. By extensive evaluation, we noticed that the classification accuracy strongly depends on the number of training samples. Table I shows the classification accuracy of both methods when using a high percentage of training samples in case of the Indian Pines database. By analysing the results from Table I, we can observe that the performance of the two operators is very similar, the improvement brought by the hyperspectral MRELBP being rather small.

TABLE I. CLASSIFICATION ACCURACY INDIAN PINES [%]

No. of training samples	Hyperspectral $LBP^{riu2}_{1,8}$	Proposed hyperspectral MRELBP
10%	96.7±0.42	**98.7±0.24**
20%	98.59±0.2	**99.65±0.1**
75%	99.82±0.08	**99.95±0.04**

However, the almost perfect precision even for a simple $LBP^{riu2}_{1,8}$ operator, is due to the fact that the same hyperspectral image is used for both training and testing. By using these hyperspectral scenes and patch-based feature vector construction, the independency between the training and test sets is not assured 100%. Even if the training and test sets are disjoint, there is a degree of overlapping between the histograms of neighbouring pixels. Due to this dependency, the classification accuracy results are not realistic for a practical application. Fig. 3 shows three histograms obtained from the $LBP^{riu2}_{1,8}$ codes for 3 pixels of the Indian Pines database at the following coordinates: (8,109), (8,110) and (41,116). All pixels belong to the same category, the Soybean-mintill, two of them being very close to each other spatially, while the other being situated in another part of the image. Table II shows the chi squared ($\chi 2$) distance [14] calculated between each pair of histograms.

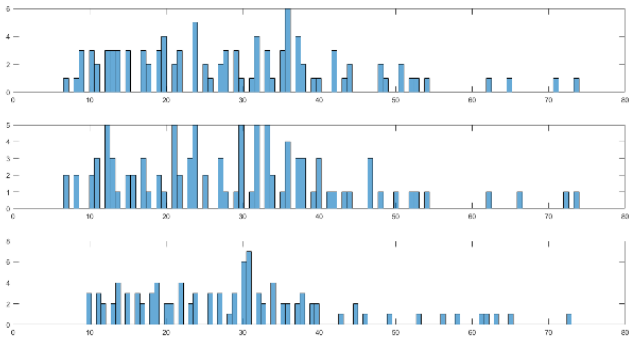

Fig. 3. Histogram example for three pixels

TABLE II. THE CHI SQUARED DISTANCE BETWEEN HISTOGRAMS

Pixels (8,109) and (8,110)	Pixels (8,109) and (41,116)	Pixels (8,110) and (41,116)
3.08	66.56	67.89

We can observe from Fig. 3 that visually, the histograms of neighbouring pixels are much more alike than the histogram of a pixel which is situated at a larger distance from them, even if all three pixels are from the same class. We can observe better this difference by analysing the $\chi 2$ distance calculated between the three histograms which is given in Table II. We can deduce that the distance is much bigger between pixels which are not neighbours. This is due to the high degree of overlap between histograms of neighbouring pixels (pixels which are situated in a neighbourhood of 17*17, this being the window used for the histogram generation). By using a high percentage of training pixels, there is an increased probability that a high number of test pixels are very close to the training ones and the dependency is not assured. In order to analyse the performance of the two methods in real world applications, the dependency between the training and test sets should be decreased. This can be done by using a smaller and fixed number of training samples, chosen randomly. In this way, the probability that those samples are close to the test samples is smaller, thus the dependency is decreased. Such an approach was taken also in [7]. For all considered hyperspectral databases, we varied the number of training samples in order to assess the operators 'performance in different situations. Table III and Table IV show the overall classification accuracy and standard deviation for the Indian Pines and SalinasA databases respectively.

TABLE III. OVERALL CLASSIFICATION ACCURACY [%] FOR THE INDIAN PINES DATABASE

Number of training samples	Hyperspectral $LBP^{riu2}_{1,8}$	Proposed hyperspectral MRELBP
3	51.57±3.43	**56.55±5.03**
5	60.96±2.41	**68.29±4.32**
10	71.98±2.29	**81.11±2.89**
13	79.8±2.13	**84.09±2.16**

TABLE IV. OVERALL CLASSIFICATION ACCURACY [%] FOR THE SALINAS A DATABASE

No. of training samples	Hyperspectral $LBP^{riu2}_{1,8}$	Proposed hyperspectral MRELBP
3	56.71±5.51	**65.14±6.61**
5	68.8±5.14	**77.4±5.38**
10	82.82±2.88	**90.3±3.2**
20	91.1±1.94	**96.67±1.2**

One can observe from Tables III and IV that the proposed classification approach surpasses the performance of the $LBP^{riu2}_{1,8}$ operator in all considered situations. By comparing the results from Table III with the ones from Table I, one can notice that the classification accuracy strongly depends on the number of training samples, as explained. For a high percentage of training samples, the improvement brought by the proposed approach was small because it was masked by the dependency between training and test sets. However, when using a smaller number of training samples, the improvement achieved by using the proposed classification method becomes

clearer and the results are more realistic for a real-world classification system.

Fig. 4 shows the confusion matrices obtained for one run on the Indian Pines database for the two feature extraction methods, Fig. 5 displays the ground truth and Fig. 6 shows the corresponding classification maps for the Indian Pines database. We can see that classes 1, 7 and 9 are easily recognized in both cases. This is because these classes have fewer samples and all of them are situated in proximity. So, there is a degree of dependence between training and testing even if fewer training samples are used. For the rest of the classes except for classes 4 and 5, the proposed approach performs better. From Fig. 6 a) and b) we can observe that the proposed approach improves the classification accuracy, as the classification map is more similar to the ground truth.

Tables V and VI show the obtained overall classification accuracies for the Salinas database and the Pavia University database respectively. We tested a higher number of training samples for these two databases because they contain much more samples than the previous ones. One can observe from these results that our proposed operator improved the classification accuracy in all considered situations.

In [7], the authors reported an overall classification accuracy and standard deviation of 61.59%±7.32 for the $LBP^{riu2}_{1,8}$ and, respectively, of 70.25%±7.63 for their proposed operator, the ST-3-D^2 LBP (the slack threshold-based 3-D dense LBP) for the Pavia University database when using 3 training samples for each class. The results are comparable to the ones obtained by us for the same database by using 9 training samples for each class. In case of the $LBP^{riu2}_{1,8}$ operator, the same parameters were used in our approach as in [7], the only difference being the number of spectral bands used. We selected and used only 10 spectral bands and the authors in [7] employed all 103 spectral bands. While they obtained the same results using less training samples, but more spectral bands, we made a compromise between computational complexity and processing times and classification accuracy.

TABLE V. OVERALL CLASSIFICATION ACCURACY [%] FOR THE SALINAS DATABASE

No. of training samples	Hyperspectral $LBP^{riu2}_{1,8}$	Proposed hyperspectral MRELBP
5	66.89±2.61	**77.74±3.58**
10	76.86±1.81	**90.07±3.2**
20	84.97±1.35	**96.5±0.99**

TABLE VI. OVERALL CLASSIFICATION ACCURACY [%] FOR THE PAVIAU DATABASE

No. of training samples	Hyperspectral $LBP^{riu2}_{1,8}$	Proposed hyperspectral MRELBP
9	61.17±3.41	**70.17±5.8**
15	67.74±3.41	**78.25±4.36**
20	71.07±2.90	**83.02±3**

Class	1	2	3	4	5	6	7	8	9	10	11	12	13	14	15	16
1	36	46	0	0	0	0	0	0	0	2	0	0	0	0	0	0
2	0	681	15	0	0	26	0	0	0	75	179	0	0	95	2	0
3	0	2	316	0	0	0	0	0	0	0	3	0	4	0	0	0
4	0	0	32	176	0	12	0	1	0	0	0	43	0	0	1	0
5	0	139	65	0	341	1	0	0	0	13	177	1	0	29	0	0
6	0	80	23	0	3	535	0	1	0	43	81	15	0	0	0	0
7	0	0	0	0	18	0	18	0	0	0	0	0	0	0	0	0
8	0	0	2	0	0	0	0	389	0	0	107	0	0	31	0	0
9	0	1	69	0	0	100	0	0	10	0	5	11	0	0	0	0
10	0	210	1	0	0	0	0	1	0	673	41	15	0	13	0	0
11	0	154	0	0	2	45	0	2	0	3	1145	0	0	14	0	0
12	0	22	18	0	0	1	0	0	0	31	25	315	0	0	0	2
13	0	0	44	0	0	0	0	0	0	0	143	0	191	27	0	0
14	0	29	0	0	0	0	0	0	0	0	300	0	0	962	0	0
15	0	6	0	0	0	0	0	0	0	5	71	1	0	4	177	0
16	0	18	0	0	0	0	0	2	0	0	0	110	0	0	0	81
no. of test samples	36	1388	585	176	364	720	18	396	10	845	2277	511	195	1175	180	83
accuracy per class	100.0%	49.1%	54.0%	100.0%	93.7%	74.3%	100.0%	98.2%	100.0%	79.6%	50.3%	61.6%	97.9%	81.9%	98.3%	97.6%
total accuracy	67.49%															

a)

Class	1	2	3	4	5	6	7	8	9	10	11	12	13	14	15	16
1	36	24	0	0	0	0	0	0	0	5	0	0	0	0	0	0
2	0	896	33	0	5	9	0	0	0	14	190	0	0	0	1	0
3	0	0	454	3	0	0	0	0	0	0	0	18	1	0	0	0
4	0	0	0	159	0	0	0	0	0	0	0	20	0	0	0	0
5	0	0	14	0	284	6	0	0	0	0	29	0	0	0	0	0
6	0	10	0	0	0	606	0	0	0	0	33	5	0	0	0	0
7	0	0	0	0	57	0	18	0	0	0	0	0	0	0	0	0
8	0	0	0	0	0	0	0	396	0	0	22	0	0	10	0	0
9	0	0	24	0	4	43	0	0	10	0	0	13	0	0	0	0
10	0	245	0	0	0	0	0	0	0	764	154	0	0	0	0	0
11	0	146	1	0	0	0	0	0	0	11	1763	0	0	120	0	0
12	0	0	0	14	0	0	0	0	0	13	0	391	0	0	0	0
13	0	0	20	0	0	0	0	0	0	0	44	0	194	0	0	0
14	0	45	0	0	0	56	0	0	0	3	0	4	0	1045	0	0
15	0	22	39	0	14	0	0	0	0	35	42	2	0	0	179	0
16	0	0	0	0	0	0	0	0	0	0	0	58	0	0	0	83
no. of test samples	36	1388	585	176	364	720	18	396	10	845	2277	511	195	1175	180	83
accuracy per class	100.0%	64.6%	77.6%	90.3%	78.0%	84.2%	100.0%	100.0%	100.0%	90.4%	77.4%	76.5%	99.5%	88.9%	99.4%	100.0%
total accuracy	81.24%															

b)

Fig. 4. Confusion matrix for one run on the Indian Pines database with 10 training samples and a)$LBP^{riu2}_{1,8}$ operator b) MRELBP algorithm

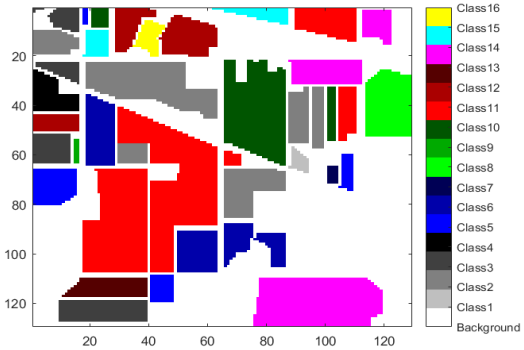

Fig. 5. Ground truth for the Indian Pines database

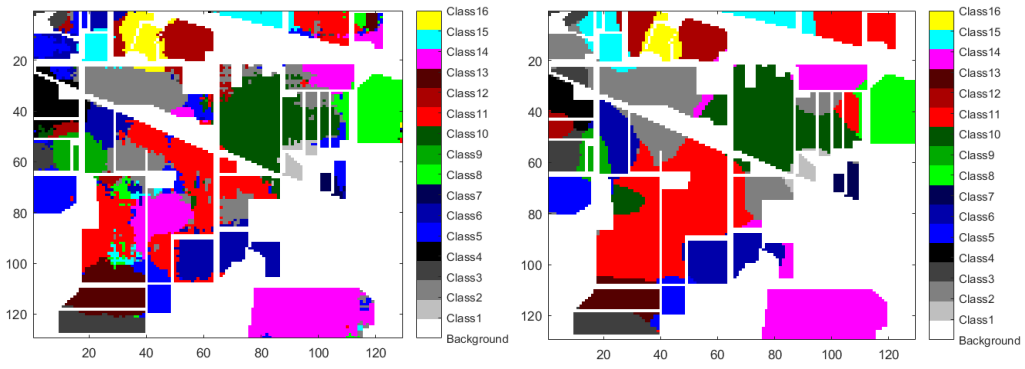

a) b)

Fig. 6. Classification map for one run on Indian Pines database with 10 training samples and a) $LBP_{1,8}^{riu2}$ operator b) MRELBP operator

V. Conclusions and Future Work

We proposed an extension to hyperspectral image classification of the MRELBP descriptor in order to combine spectral and spatial information for more discrimination power. We showed that for decreasing the dependency between training and test sets, a small number of training samples should be used to analyse the real performance of feature extraction methods. We evaluated our method in comparison to the rotation invariant uniform LBP on four different hyperspectral databases and we achieved improvements in classification performance.

As future work, we plan to further improve the classification performance by using the BM3DELBP (Block Matching and 3D Filtering Extended Local Binary Pattern) operator [15].

The proposed feature extraction method solves a fundamental problem and can work with hyperspectral images from several research areas such as precision agriculture and medical imaging. In fact, the proposed technique was developed for a bio-engineering application, for the identification of diseases for hyperspectral images of vineyards. We are currently acquiring a database of hyperspectral images of healthy and unhealthy grape leaves and vineyard parcels. We plan to test the proposed algorithms for the classification of different diseases affecting grape leaves by using different images for training and tests in order to avoid any dependency between the two sets and asses the performance of the proposed algorithms in a real-life scenario. We also intend to test the performance of the proposed approach on medical hyperspectral images.

Acknowledgment

This work was supported by a grant of the Romanian Ministry of Research and Innovation, CCCDI-UEFISCDI, project number PN-III-P1-1.2-PCCDI-2017-0251/4PCCDI/ 2018, within PNCD III.

References

[1] T. Ojala, M. Pietikäinen and D. Harwood, “A comparative study of texture measures with classification based on feature distributions”, Pattern Recognition, vol. 29, pp. 51-59, January 1996.

[2] T. Ojala, M. Pietikainen and T. Maenpaa, “Multiresolution gray-scale and rotation invariant texture classification with local binary patterns”, IEEE Trans. Pattern Anal. Mach. Intell, vol. 24, pp. 971–987, July 2002.

[3] L. Li, L. Zhao, Y. Long, G. Kuang and P. Fieguth, “Extended local binary patterns for texture classification”, Image and Vision Computing, vol. 30, pp. 86-99, February 2012.

[4] L. Liu, S. Lao, P. W. Fieguth, Y. Guo, X. Wang and M. Pietikäinen, “Median Robust Extended Local Binary Pattern for Texture Classification”, IEEE Trans. Image Processing, vol. 25, pp. 1368-1381, March 2016.

[5] L. Paulhac, P. Makris and Jean-Yves Ramel, “Comparison between 2D and 3D Local Binary Pattern Methods for Characterisation of Three-Dimensional Textures”, Image Analysis and Recognition: 5th International Conference, pp. 670-679, June 2008.

[6] J. Fehr and H. Burkhardt, “3D Rotation Invariant Local Binary Patterns”, 2008 19th International Conference on Pattern Recognition, January 2009.

[7] Sen Jia, Jie Hu, Jiasong Zhu, Xiuping Jia, Qingquan Li, “Three-Dimensional Local Binary Patterns for Hyperspectral Imagery Classification”, IEEE Transactions on Geoscience and Remote Sensing,vol. 55, pp. 2399-2413, April 2017.

[8] Sen Jia, Jie Hu, Lin Deng, Xiuping Jia, “Three-dimensional local binary patterns for hyperspectral imagery classification”, 2016 IEEE International Geoscience and Remote Sensing Symposium, November 2016.

[9] Wei Li, Chen Chen, Hongjun Su, Qian Du, “Local Binary Patterns and Extreme Learning Machine for Hyperspectral Imagery Classification”, IEEE Transactions on Geoscience and Remote Sensing, vol. 53, pp. 3681 – 3693, July 2015.

[10] Junjun Jiang , Jiayi Ma, Chen Chen, Zhongyuan Wang, Zhihua Cai, Lizhe Wang, “SuperPCA: A Superpixelwise PCA Approach for Unsupervised Feature Extraction of Hyperspectral Imagery”, IEEE Transactions on Geoscience and Remote Sensing, vol. 56, pp. 4581 – 4593, August 2018.

[11] Huizhen Yang, Feng Gao, Junyu Dong, Yang Yang, “Hyperspectral image classification based on local binary patterns and PCANet”, Proc. SPIE 10615, Ninth International Conference on Graphic and Image Processing (ICGIP 2017), October 2017.

[12] Christopher J. C. Burges, “A Tutorial on Support Vector Machines for Pattern Recognition”, Data Mining and Knowledge Discovery, pp. 121-167, June 1998.

[13] ”Hyperspectral Remote Sensing Scenes”, Internet: http://www.ehu.eus/ccwintco/index.php/Hyperspectral_Remote_Sensing_Scenes, [May 24,2019].

[14] Y. Rubner, C. Tomasi and L. J. Guibas, “The Earth Mover's Distance as a Metric for Image Retrieval”, International Journal of Computer Vision, vol. 40, pp. 99-121, November 2000.

[15] S. R. Barburiceanu, S. Meza, C. Germain, R. Terebes, "An Improved Feature Extraction Method for Texture Classification with Increased Noise Robustness", 27th European Signal Processing Conference, pp. 2082-2086, September 2019.